

---

# Field Test and Structural Stability Analysis of Multi-stage Slope Based on Seepage Coupling Theory

---

Lu Hao\*, Li Qing and Li Peijun

*Guangdong Transportation Technology Testing Co.,Ltd., Guang Zhou Guangdong 510550, China*

*E-mail: lhchd0220@126.com*

*\*Corresponding Author*

Received 24 May 2023; Accepted 04 July 2023;

Publication 30 September 2023

## **Abstract**

This study takes the slope engineering of the Guangdong North Expressway as the background, and studies the impact of rainfall infiltration on the stability of high slopes through on-site monitoring, data analysis, and model construction. Firstly, based on BC theory, the mechanical calculation model of landslide rainfall is established, and the mechanical formula of slope mechanical properties and Factor of safety considering rainfall process and rainfall infiltration process is derived. Then, by constructing a Fluid–structure interaction numerical calculation model considering the seepage characteristics and mechanical state evolution of the slope, the movement of pore water in the slope under different rainfall intensities and the evolution of the mechanical state and displacement characteristics of the slope were studied. Research has found that the mechanical and numerical calculation models in this article are highly consistent with the actual site conditions, and there may be two potential sliding surfaces in the K738+995 section. The potential sliding surface of K738+910 section is located at a depth of 7 m below the first level platform and 3 m below the third level platform; There may be two

*European Journal of Computational Mechanics, Vol. 32\_3, 235–262.*

doi: 10.13052/ejcm2642-2085.3232

© 2023 River Publishers

potential sliding surfaces in K738+658 section, one is located at the interface between silty clay and sandy clay (9 m below the top of cutting), and the other is mainly located at the interface between sandy clay and completely weathered andesite porphyrite; The surface layer of the slope is silty clay and sandy clay, and the underlying layer is fully strongly weathered andesite porphyrite and moderately weathered dacite. Completely strongly weathered andesite porphyrite is soft, easy to soften and disintegrate when encountering water, and joint fissures are developed. The surface of some cracks is contaminated with iron and manganese, resulting in uneven weathering. The rock is relatively soft and the rock mass is broken. Due to the recent continuous heavy rainfall, the water content of the surface soil of the slope gradually increases and tends to saturation, increasing the self-weight of the slope soil.

**Keywords:** Highway slope, mechanical calculations, mechanical properties, mechanical performance, risk analysis.

## 1 Introduction

Rainfall infiltration causes shallow slope collapse and instability, which not only causes property losses and casualties, but also affects social stability and production and construction activities [1, 2]. Rainfall, especially rainstorm, becomes the most important inducing factor of slope failure. During rainfall, due to an increase in soil moisture content, the effective stress between matrix suction and soil particles decreases, resulting in a decrease in soil shear strength and causing slope instability. There are various classification methods for soil landslides, for example, they can be classified based on the scale of the landslide, the age of landslide formation, the movement characteristics of the landslide, and the dynamic causes [3, 4]. Rainfall type landslides have the characteristics of mass occurrence and chain generation, and have strong disaster causing ability. Landslides, as a common and frequent geological hazard, are more common in engineering construction such as water conservancy, transportation, civil engineering, and mining. Domestic and foreign experts unanimously believe that rainfall is the main cause of landslides, especially long-term heavy rainfall, which can easily lead to landslide disasters [5, 6]. In the southern region of China, there are many mountainous areas, complex terrain, long rainy seasons, and high rainfall. Landslides containing weak interlayers are prone to softening and rapidly reducing their shear strength under the action of rainfall infiltration, leading to landslide disasters. According to statistics, about 30% of geological disasters

in China occur every year in soil plateau areas that account for less than 5% of the country's land area, and are concentrated in the rainy season from June to October, Water is one of the most active inducing factors for soil landslides [7, 8]. The South China region has a wide soil coverage area and a large accumulation thickness, with numerous soil ridges and gullies. Soil erosion is relatively severe, and the region belongs to a temperate continental monsoon climate with an average annual rainfall of 562 mm, mainly distributed in autumn. The fragmented terrain and special natural climate conditions, as well as the unreasonable use of natural resources by humans in recent years, have led to a high and frequent occurrence of landslides and collapses, posing serious harm [9, 10]. Slope stability is relative and temporary. Even slopes that are currently in a stable state will gradually develop from a stable state to an unstable state under long-term adverse factors such as manual excavation, earthquakes, rainfall, etc., leading to various geological disasters such as landslides and landslides [11, 12].

In order to obtain a more accurate transient seepage field under rainfall infiltration conditions, it is necessary to establish appropriate mathematical models and reliable unsaturated seepage hydraulic characteristic parameters [13, 14]. The Richards equation has high computational accuracy in studying soil moisture movement, but its application is often limited due to its non-linear characteristics. Previous studies have typically used finite element and finite difference numerical methods to solve unsaturated seepage problems [15, 16]. Although these methods can largely compensate for the limitations of previous studies, However, it requires a higher level of understanding of engineering geology and external constraints, often making it difficult to obtain many parameters, which also leads to the application of such methods only as an auxiliary. In 1856, French hydraulic scientist Darcy obtained the famous Darcy's law by analyzing the results of one-dimensional seepage experiment of sand; In 1889, Zhukovsky first proposed a homogeneous, simple boundary saturated seepage differential equation through theoretical derivation; Richards combined Darcy's law with continuum equation to derive three-dimensional differential equation describing soil seepage; Horton proposed an empirical model through the analysis and research of a large amount of experimental data [17, 18], and thus the relevant research methods have been developed comprehensively. However, the application of the above methods is currently mostly based on a single method, without systematic comparative application.

In response to the shortcomings of the previous research, this study relied on a highway slope project in northern Guangdong, combined with three

commonly used methods such as on-site monitoring, data processing and analysis, and model construction, to explore the impact of rainfall infiltration on the stability of high slopes. On this basis, the analytical formula of slope Factor of safety considering the redistribution of wet layer during rainfall is derived, and the Fluid–structure interaction numerical calculation model considering the seepage characteristics of the slope is established. Through numerical simulation, the movement of pore water and the evolution of slope displacement under different rainfall intensities are studied. Related research not only systematically studies the impact of rainfall infiltration on the stability of high slopes, but also combines the application of different methods. It has strong theoretical and practical significance.

## 2 Slope Rainfall Mechanics Model Based on Improved Green Ampt Formula

As rainfall continues, the dominant factors of rainwater infiltration will change. The rainwater infiltration process can be divided into two stages: the early rainfall stage and the accumulated water infiltration stage [19, 20]. The dominant factors in the two stages are rainfall intensity and soil infiltration capacity. (1) Early rainfall stage: In the early stage of rainfall, the rainfall intensity is less than the infiltration rate of the slope, and all rainwater seeps into the interior of the slope [21, 22]; (2) Stages of water accumulation and infiltration: As rainfall continues, the slope surface gradually becomes saturated, the permeability coefficient of the soil gradually decreases, and water accumulation begins to form on the slope surface [23, 24]. The dominant factor changes from rainfall intensity to the infiltration capacity of the soil, and the calculation diagram of rainwater infiltration is shown in Figure 1 when the slope conditions decrease.

### (1) Early rainfall stage

As shown in Figure 1, under slope conditions, the rainfall intensity on the vertical slope is  $p = q * \cos\alpha$ , The infiltration rate  $i$  of the soil at this stage is controlled by the intensity of rainfall, therefore [25, 26]:

$$i_1 = p \quad (1)$$

The rainfall infiltration amount  $I'_1$  in the saturated zone during this stage is:

$$I'_1 = z_{s1} \cdot (\theta_s - \theta_i) \quad (2)$$

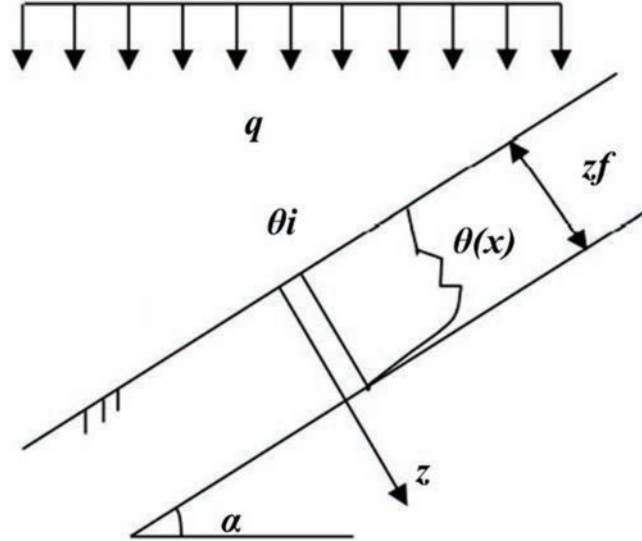


**Figure 1** Schematic diagram of rainfall infiltration calculation under slope conditions.

To obtain the distribution of water content at any depth in the unsaturated transition zone, based on the soil water characteristic curve, the model proposed by Brooks and Corey (abbreviated as BC model) in 1980 was selected as the calculation model for this study, namely [27, 28]:

$$S_e = \frac{\theta - \theta_r}{\theta_s - \theta_r} = \left(\frac{s_a}{s}\right)^n \quad (3)$$

By combining the above two equations, the rainfall infiltration amount in the unsaturated transition zone is:

$$I_2 = \int_{z_{s1}}^{z_{f1}} [\theta(z) - \theta_i] dz = (z_{f1} - z_{s1}) \cdot \left[ (\theta_r - \theta_i) + \frac{(\theta_s - \theta_r)}{1 - n} \left(\frac{s_a}{s_f}\right)^n \right] \quad (4)$$

The total infiltration amount  $I_1$  during the early rainfall infiltration stage is:

$$I_1 = I_1 + I_2 = z_{s1} \cdot (\theta_s - \theta_i) + (z_{f1} - z_{s1}) \cdot \left[ (\theta_r - \theta_i) + \frac{(\theta_s - \theta_r)}{1 - n} \left(\frac{s_a}{s_f}\right)^n \right] \quad (5)$$

$t_1 = I_1/i_1$ , therefore:

$$t_1 = \frac{I_1}{i_1} = \frac{z_{s1} \cdot (\theta_s - \theta_i) + (z_{f1} - z_{s1}) \cdot \left[ (\theta_r - \theta_i) + \frac{(\theta_s - \theta_r)}{1-n} \left( \frac{s_a}{s_f} \right)^n \right]}{p} \quad (6)$$

## (2) Water infiltration stage

After experiencing the early stage of rainfall infiltration, the slope gradually becomes saturated, and the boundary conditions change, entering the stage of water accumulation infiltration [29, 30]. The infiltration capacity of the soil at this stage is mainly controlled by the infiltration rate of the soil. When the Green-Ampt model is applied under slope conditions, according to Darcy's law, the total head difference is  $z_f \cos \alpha$ , the matrix suction of the moist front is  $s_0$ , and the seepage path is  $z_f$ .

- (1) When water accumulates on the slope, the rainfall intensity  $p$  along the normal direction of the slope is equal to the infiltration rate  $i$  of the soil, and the depth of water accumulation  $H = 0$ .

$$i_p = p = k_s \frac{z_p \cos \alpha + h_f}{z_p} \quad (7)$$

The expression for the depth of the wetting front at the onset of water accumulation is:

$$z_{fp} = \frac{k_s h_f}{p - k_s \cos \alpha} \quad (8)$$

Similarly, at this time, the total infiltration amount and infiltration time of rainwater in the normal direction of the slope are:

$$I_p = z_{sp} \cdot (\theta_s - \theta_i) + (z_{fp} - z_{sp}) \cdot \left[ (\theta_r - \theta_i) + \frac{(\theta_s - \theta_r)}{1-n} \left( \frac{s_a}{s_f} \right)^n \right] \quad (9)$$

- (2) After the accumulation of water on the slope, the rainfall intensity  $p$  on the vertical slope is greater than the infiltration rate of the soil. At this point, the infiltration rate  $i_2$  of the soil is:

$$i_2 = k_s \frac{z_{f2} \cos \alpha + h_f}{z_{f2}} \quad (10)$$

According to the principle of water balance, at any given moment, the surface infiltration flux  $q$  in  $dt$  should be equal to the sum of the moisture increments in the moist layer of the soil, i.e. [31, 32]:

$$i_2 \cdot dt = dz_{s2} \quad (11)$$

The rainfall infiltration time for the above two stages of rainfall and water infiltration is:

$$t = \begin{cases} \frac{z_s \cdot (\theta_s - \theta_i) + (z_f - z_s) \cdot \left[ (\theta_r - \theta_i) + \frac{(\theta_s - \theta_r)}{1-n} \left( \frac{s_a}{s_f} \right)^n \right]}{q \cos \alpha}, & t \leq t_p \\ t_2 = \frac{\lambda(\theta_s - \theta_i) + (1 - \lambda) \left[ \theta_r - \theta_i + \frac{(\theta_s - \theta_i)}{1-n} \cdot \left( \frac{s_a}{s_f} \right)^n \right]}{k_s} \\ \cdot \left[ z_{f2} - s_f \ln \frac{z_{f2} + s_f}{s_f} \right], & t > t_p \end{cases} \quad (12)$$

### 3 Mechanical Model of Slope Safety Coefficient Based on Seepage Theory

In general, landslides caused by rainfall are shallow landslides, characterized by a sliding surface parallel to the surface of the slope [33–35]. Therefore, stability analysis can be conducted assuming it is an infinite slope. The infinite slope stability calculation model is shown in Figure 2.

According to Figure 2, the tangential component of the sliding soil along the sliding surface is:

$$\tau = \gamma_t z_w \cos \beta \sin \beta = \gamma_t z_f \sin \beta \quad (13)$$

According to Fredlund's unsaturated shear strength theory, the sliding resistance is:

$$\tau_f = c' + (\sigma_n - u_a) \tan \varphi' + (u_a - u_w) \tan \varphi^b \quad (14)$$

From Equations (13) and (14) above, the safety factor  $F_s$  of the slope can be obtained as:

$$F_s = \frac{\tau_f}{\tau} = \frac{c' + (\gamma_t z_f \cos \beta - u_a) \tan \varphi' + (u_a - u_w) \tan \varphi^b}{\gamma_t z_f \sin \beta} \quad (15)$$



in Equation (19) as follows:

$$F_s = \frac{c' + \left\{ (1 + \theta_s) \cdot \lambda + (1 - \lambda) \cdot \left[ 1 + \theta_r + \frac{(\theta_s - \theta_r)}{1-n} \left( \frac{s_a}{s_f} \right)^n \right] \right\} \cdot z_f \cdot \gamma_d \cdot \cos\beta \cdot \tan\varphi' - u_w \cdot \tan\varphi^b}{\left\{ (1 + \theta_s) \cdot \lambda + (1 - \lambda) \cdot \left[ 1 + \theta_r + \frac{(\theta_s - \theta_r)}{1-n} \left( \frac{s_a}{s_f} \right)^n \right] \right\} \cdot z_f \cdot \gamma_d \cdot \sin\beta} \quad (19)$$

#### 4 Field Monitoring and Mechanical Performance Analysis of Highway High Slopes

Affected by continuous heavy rainfall, the high slope on the right side of the southbound section of Renxin Expressway K738+586~K739+156 (design mileage K288+850~K289+420) suffered from water damage. The landslide was cut out from the foot of the slope and the upper part cracked, seriously threatening the normal operation of the expressway. It is urgent to carry out slope monitoring and stability analysis based on on-site engineering geological conditions.

##### 4.1 Project Overview

The panoramic view and zoning of the landslide area are shown in Figure 3. The slope length of this section is relatively large, and it is divided into three areas based on the slope characteristics and deformation characteristics, namely Zone 1, Zone 2, and Zone 3. The groundwater in the site mainly includes two types: Quaternary pore phreatic water and bedrock fissure water. Quaternary pore phreatic water mainly occurs in gravelly silty clay, completely weathered, sandy strongly weathered Andesite porphyrite, and bedrock fissure water mainly occurs in fragmentary strongly weathered argillaceous Siltstone fissures. The natural slope at the top of the cutting has a large surface catchment area, poor surface runoff conditions, and surface water is easy to recharge groundwater. Partially weathered and sandy strongly weathered Andesite porphyrite has high clay mineral content, which is easy to isolate water. This leads to poor permeability of the slope rock mass, making it difficult for groundwater to discharge smoothly downwards, resulting in deformation of the slope along the weak structural plane. The groundwater on the site is directly supplied by atmospheric precipitation and has obvious seasonal characteristics. At present, the groundwater on the slope is very abundant, and the bleeding in the landslide area is very serious. The water



**Figure 3** Overview and zoning of landslide area.



**Figure 4** Cracking of on-site slope and platform.

output of the inclined drainage hole on the slope is very high. The groundwater on the site is directly supplied by atmospheric precipitation and has obvious seasonal characteristics. At present, the groundwater on the slope is very abundant, and the bleeding in the landslide area is very serious. The water output of the inclined drainage hole on the slope is very high. The cracks on the site slope and platform are shown in Figure 4.

Based on the comprehensive on-site slope disaster investigation data, it can be concluded that the deformation in Zone I mainly occurs above the second level platform, and the deformation below the second level is relatively small. There is some deformation in the low foot wall and side ditch at the foot of the slope, but the deformation is relatively small. Combined with the monitoring of high slopes, the thickness of the landslide is about 14 m, the length is 126 m, the width is about 200 m, and the volume of the landslide is about  $25 \times 10^4 \text{ m}^3$ , with poor slope stability and in an ultimate stable state. The deformation in Zone II is mainly concentrated within a range of 80 m near the junction with Zone III. The low foot wall and side ditch at the foot of the slope are severely tilted outward, and emergency pier bag back pressure is carried out in the later stage. The first and second level platforms have severe cracks, while the third level platform has tensile cracks. The cracks are not obvious on the anchor cable frame slope surface. According to geological survey and deep hole monitoring, the thickness of the landslide body is about 14 m, the length is 126 m, the width is about 90 m, and the volume of the landslide body is about  $15 \times 10^4 \text{ m}^3$ , with poor slope stability and in an ultimate stable state. The deformation in Zone III is the most severe. The low foot wall and side ditch at the foot of the slope are severely tilted outward, and emergency pier bag back pressure is carried out in the later stage. The first level, second level, third level, and fourth level platforms are severely cracked, and the left boundary of the landslide is cracked through. The natural slope at the top of the slope is severely pulled and staggered. According to geological surveys and deep hole monitoring, the thickness of the landslide body is about 15 m, length is 125 m, width is about 125 m, and the volume of the landslide body is about  $25 \times 10^4 \text{ m}^3$ , with poor slope stability and in a state of extreme equilibrium to instability.

Based on the analysis of the current deformation status of the slope, the geological conditions of the slope engineering, and the structure of the protection and reinforcement engineering, the main reasons for the deformation of the slope are as follows: (1) Affected by continuous heavy rainfall weather, the groundwater level of the slope rises rapidly, the rock and soil on the slope become saturated, and the shear strength of the rock and soil decreases rapidly, leading to the occurrence of slope diseases; (2) The top of the slope is relatively flat, with poor surface runoff conditions. A large amount of surface water supplies groundwater, leading to the occurrence of slope diseases; (3) The development of joint cracks in the slope, intense weathering of the rock mass, and large thickness of complete weathering and sandy soil like strong weathering are one of the geological foundations for the

occurrence of slope diseases; (4) The height of the slope is relatively high. After excavation, under the influence of external forces, the rock and soil joints and fissures of the slope further open, forming vertical and horizontal water channels, providing favorable conditions for rapid infiltration of surface water to recharge groundwater. However, groundwater is also affected by the relative impermeability of weak interlayers and the high content of clay minerals. Its water level discharges slowly and rises rapidly, which increases the dynamic and static water pressure of the landslide body, reduces the effective stress of the landslide body, and leads to the occurrence of slope diseases.

#### 4.2 Field Testing and Result Analysis of Slope Mechanical State

The surface displacement monitoring of the slope was carried out by setting up 2 benchmark network buried stone points, 26 surface displacement monitoring points, 4 settlement points on the left shoulder, and 18 inclinometer holes on 5 sections. The layout of measurement points for each monitoring item is shown in Figure 5.

##### 4.2.1 Analysis of deep displacement test results

The deep displacement test results of K738+650 (Zone 1) section are shown in Figure 6.

From the analysis in Figure 6, it can be seen that there are currently three inclination measuring holes in this section. The original third level platform



Figure 5 Layout of on-site monitoring points for slope.

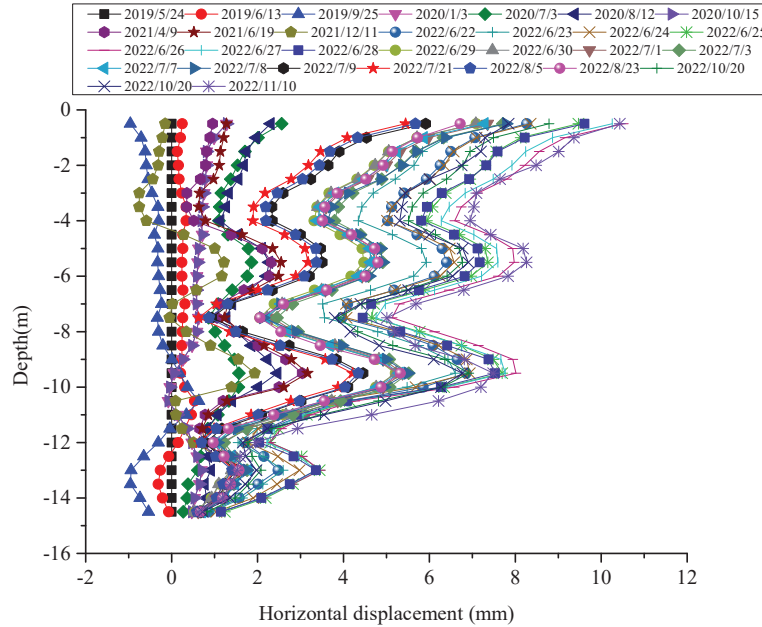
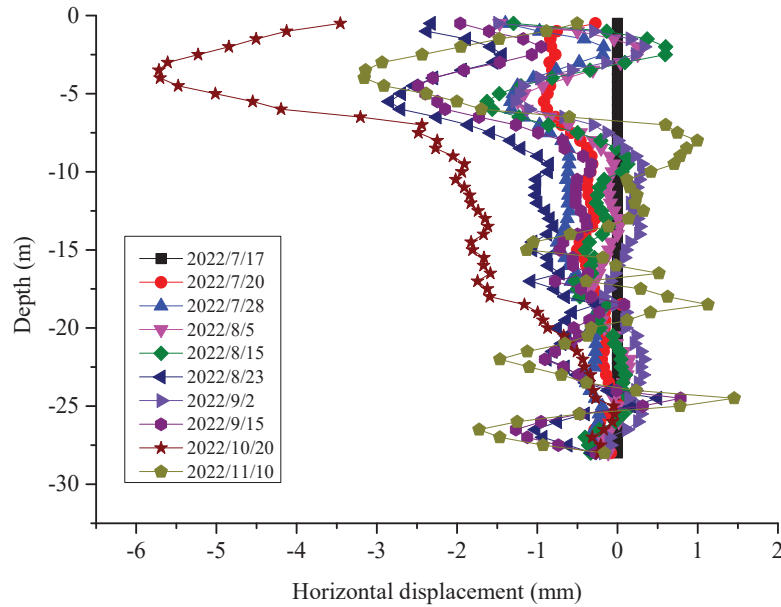


Figure 6 Deep horizontal displacement curve of cutting top.

inclination measuring holes are stuck at a depth of 9 meters, and according to previous data, they have already undergone shearing at a depth of 9 meters; We are now adding new holes on the same section of the first and fourth level platforms. At present, during the grouting construction in this area, the holes of the first and fourth level platforms have been covered up. On October 20, 2022, the cumulative maximum vertical horizontal displacement of the inclined hole at the top of the cutting was 7.84 mm (0.5 m from the hole opening), and there was no significant change compared to August 23, 2022. According to the displacement curve, there was a certain displacement from the depth of 12 mm to the top of the hole. The deep horizontal displacement test results of the first level platform of K738+910 (Zone 3) section are shown in Figure 7.

As shown in Figure 7, there are currently two inclinometer holes, with the original primary platform at a depth of 7 meters and the tertiary platform stuck at a depth of 3 meters; Further monitoring is being carried out near the first and third level platforms (which have been damaged by construction), and a new inclinometer hole is being added on the lower slope. There is no significant change in the vertical displacement of the No. 4 inclined



**Figure 7** Deep horizontal displacement curve of K738+910 primary platform.

hole on the lower slope compared to the previous period; The cumulative maximum displacement of the inclined hole in the vertical direction of the first level platform is 99.34 mm (at a depth of 3.5 m), which has not changed significantly since September 15, 2022. According to the displacement curve, there is significant displacement from the depth of 13 mm to the top of the hole. The deep horizontal displacement results of the first and third level platforms of K739+050 (Zone 3) section are shown in Figures 8 and 9.

From Figures 8 and 9, it can be seen that the monitoring of the slope in this period is as follows (arranged from bottom to top): On October 20, 2022, the cumulative maximum vertical displacement of slope 1 inclined hole, slope 2 inclined hole, and slope 3 inclined hole did not exceed 12.71 mm (depth 3.5 m), 8.64 mm (depth 0.5 m), and 5.35 mm (depth 1 m), respectively, with an increase of 3.61 mm compared to before September 15, 2022, and there was no significant change in the latter; Accumulated maximum displacement in the vertical direction. According to the displacement curve, the lower slope of section K739+050 is in the stage of creep deformation. The cumulative maximum displacement of the inclined hole at the top of the cutting in the vertical direction is 14.02 mm (0.5 meter deep), which has not changed significantly compared to the previous period on August 23, 2022.

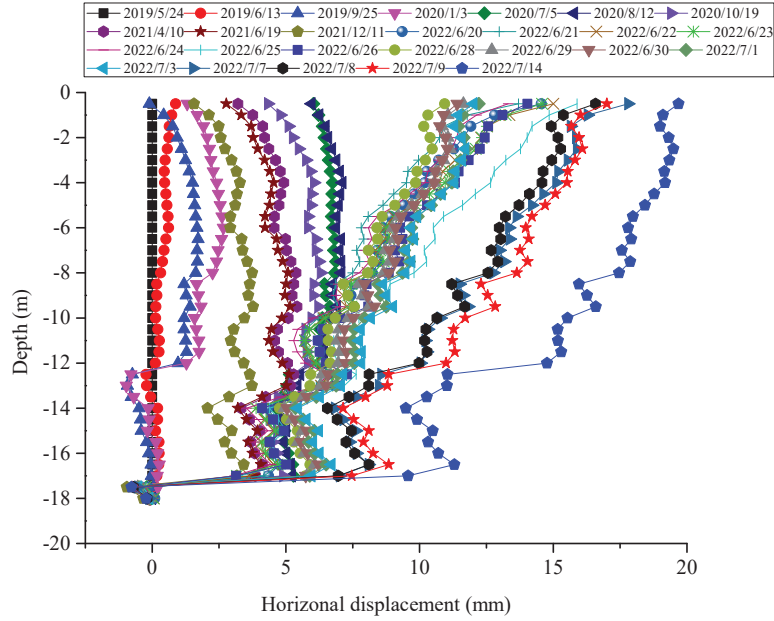


Figure 8 K739+050 deep horizontal displacement curve of the first stage platform.

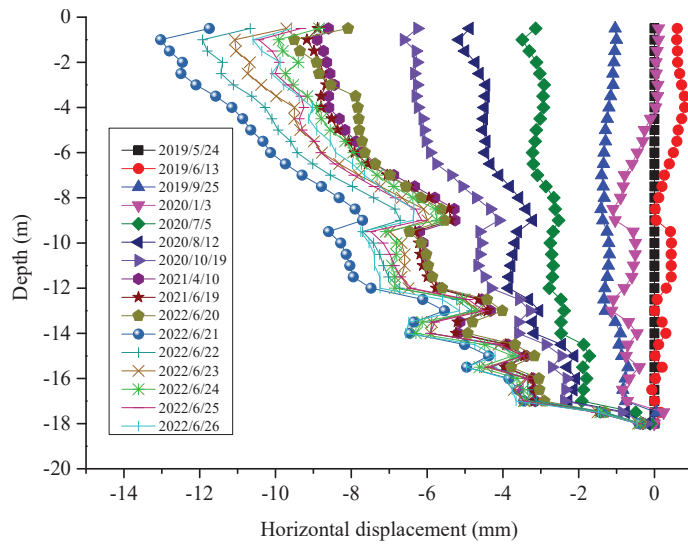


Figure 9 K739+050 horizontal displacement time history curve of the third stage platform.



**Figure 10** K738+915~K739+156 section III platform perspective and inclinometer pipe layout.

According to the displacement curve, there is a certain displacement from a depth of 22 mm to the top of the hole, and the upper displacement is relatively large.

#### **4.2.2 Analysis of surface displacement test results**

The perspective of the third level platform and the layout of the inclinometer tube for K738+915~K739+156 sections are shown in Figure 10. The cumulative lateral horizontal displacement of K738+915~K739+156 section is shown in Figure 11.

From the analysis in Figure 11, it can be seen that there has been no significant development at the measurement points of K739+060 and K739+000 sections since July 8, 2022; The A05 measuring point of the first level platform of K738+940 section was blocked after July 30, 2022, and the third level platform C03 has not developed significantly since July 8, 2022, which is tentatively considered as a construction impact; In summary, there has been no significant development of surface displacement in this area since July 8, 2022 (currently under grouting construction in this area). The cumulative lateral horizontal displacement of K738+586~K738+725 section is shown in Figure 12.

The surface displacement monitoring data shows that the cumulative lateral displacement of the K738+650 section surface displacement measurement point E-1 on October 22, 2022 is 48.7 mm, an increase of 10 mm compared to the previous period (September 17, 2022/); The cumulative lateral displacement of point C-2 is 37.4 mm, an increase of 23.3 mm compared to the previous period (September 17, 2022/); The cumulative

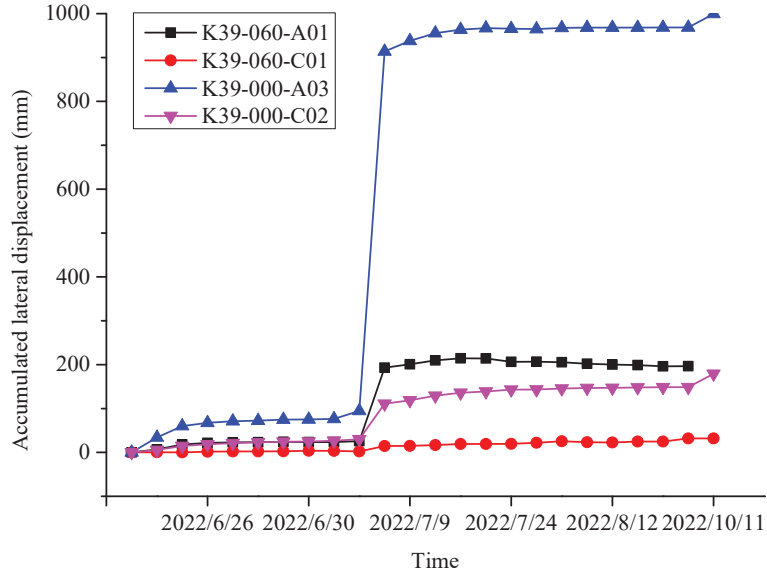


**Figure 11** Accumulated lateral horizontal displacement of K738+915~K739+156 section.

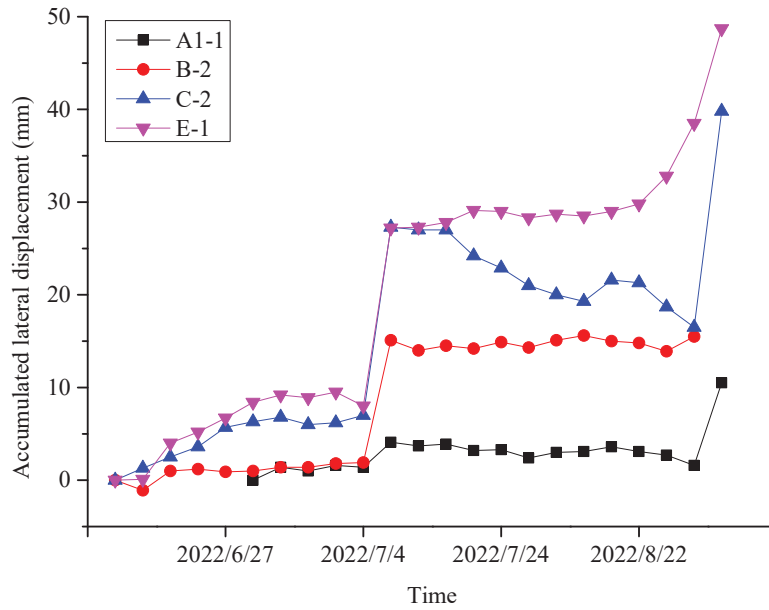


**Figure 12** Cumulative horizontal displacement of K738+650 section.

lateral displacement of A1-1 is 10.5 mm, an increase of 9 mm compared to the previous period; The B-2 measuring point was damaged.

### 4.3 Slope Mechanical Stability Analysis Based on Numerical Calculation

The finite element method is used to verify the limit equilibrium method underwater slope calculation formula obtained through theoretical derivation. The judgment method for calculating slope stability using finite element method is as follows: (1) The non convergence of finite element calculation is used as the judgment basis for slope instability; (2) Based on the occurrence of inflection points in the displacement of feature points as the judgment basis; (3) Based on the occurrence of plastic penetration zone as the judgment basis. However, there are many cases of non convergence in finite element calculation, including insufficient mesh accuracy, poor mesh quality, and unreasonable convergence conditions, which can lead to non convergence in finite element calculation. Therefore, the applicability of the method of judging whether a slope is unstable based on the convergence of finite element calculation is poor. Using the displacement inflection point of characteristic points as the basis for slope instability has clear physical significance. The stability calculation of this landslide is mainly based on back calculation parameters, combined with relevant experiments and empirical parameters to comprehensively determine the rock and soil mechanical indicators of the sliding zone. Therefore, the slope engineering professional software widely used at home and abroad is used for landslide stability calculation, specifically using the relatively strict rigid body limit equilibrium method – Morgenstein&Price method, Substitute the above formula for calculating slope safety factor and rainfall infiltration time into the software for calculation and analysis. The rainfall calculation model of high slope is shown in Figure 13, and the distribution of pore water pressure with depth under different rainfall intensities is shown in Figure 14.

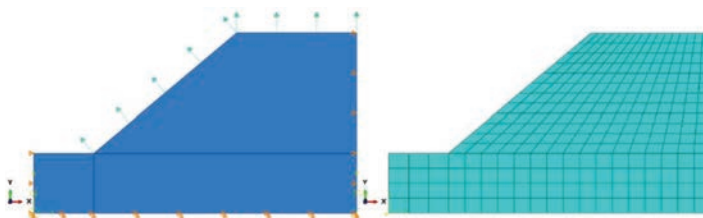


**Figure 13** Calculation model for high slope landslide seepage.

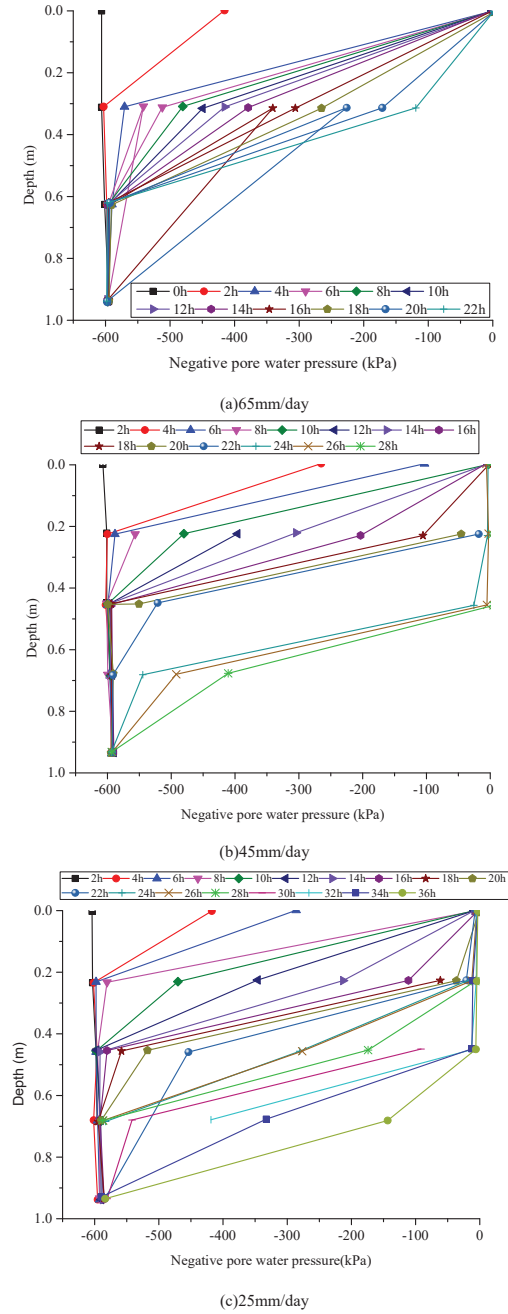


**Figure 14** Pore water pressure distribution with depth under different rainfall intensity conditions.

From Figure 14, it can be seen that under the three rainfall intensity conditions, the variation trend of pore water pressure at the top of the slope is basically consistent, and gradually increases with the increase of rainfall duration. Under the working condition of 80 mm/d rainstorm, the pore water pressure on the slope top increased to 0 in the second hour, and the slope top reached saturation in only two hours. The depth of rainfall impact reached 0.25 m in the third hour and 0.5 m in the twelfth hour. It can be seen that for different depths of soil layers, the increase rate of pore water pressure slows down with the increase of seepage path; Under heavy rain conditions of 45 mm/d, it takes 12 hours for the slope to saturate. At the 16th and 56th hours, the depth affected by rainfall reached 0.25 m and 0.5 m respectively. The soil layer below the slope top reached saturation at 0.25 m in the 18th hour, and at the 112th hour, the depth affected by rainfall reached 0.75 m. The area below the slope top reached saturation at 0.5 m in the 24th hour; Under moderate rainfall conditions of 20 mm/d, slope saturation takes 16 hours. At the 16th and 24th hours, the depth affected by rainfall reached 0.25 m and 0.5 m. At the 32nd hour, the soil layer below the slope top reached saturation at 0.25 m, and at the 36th hour, the soil layer below the slope top reached saturation. The distribution of pore water pressure and vertical displacement on slopes under different rainfall rates is shown in Figures 15 and 16.

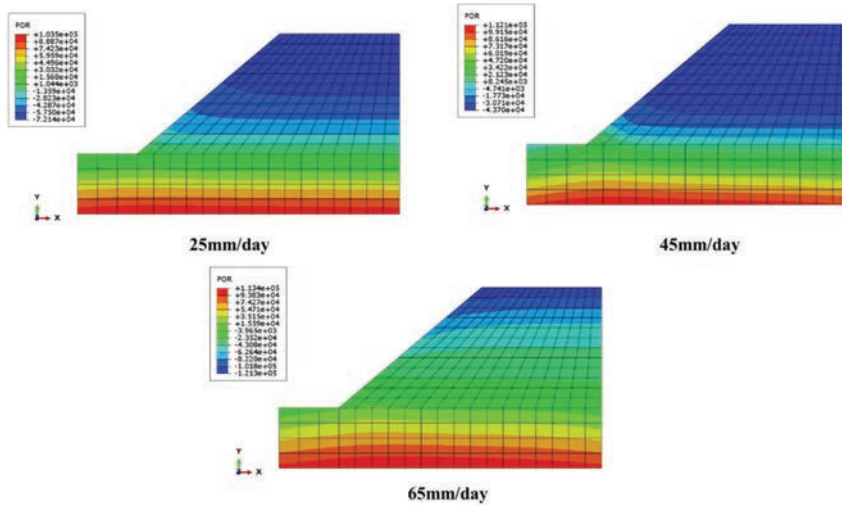


Figure 15 Distribution of pore water pressure in slopes under different rainfall rates.

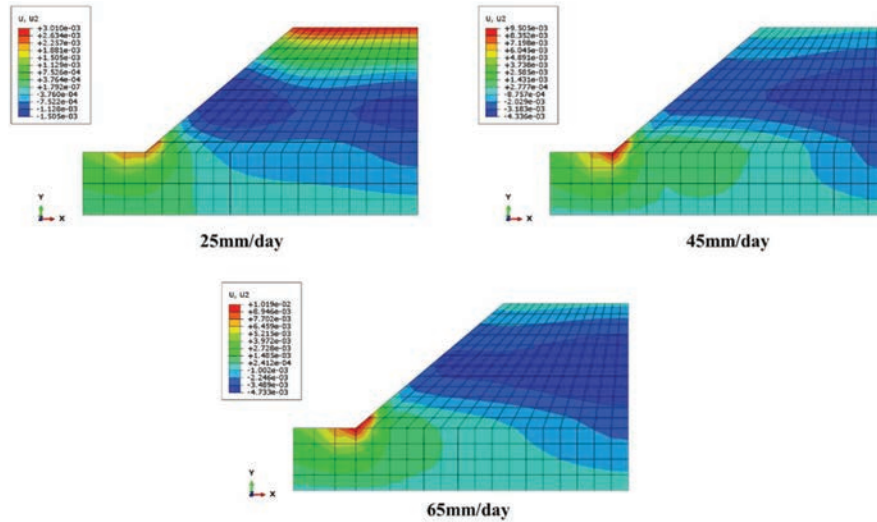


Figure 16 Vertical displacement distribution of slope under different rainfall rates.

As shown in Figures 15 and 16, when the rainstorm lasts for two days, 65 mm/d, the pore water pressure increases rapidly, and the slope top surface has reached saturation state. The distribution form of seepage field is dense at the top and sparse at the bottom. When it rains for two days, the distribution form of seepage field is dense at the bottom and sparse at the top. This is because the surface soil mass quickly reaches saturation in a short time under the effect of heavy rainfall, and then the boundary conditions are controlled by the permeability coefficient of the slope soil mass. Moreover, the saturated permeability coefficient of soil is very small, only 0.038 m/d, so the distribution characteristics of the seepage field of surface soil on the slope under the short-term rainstorm condition change with the rainfall duration from dense at the top to sparse at the bottom to dense at the bottom; Under the working condition of heavy rain of 45 mm/d for 6 days, due to the relatively high rainfall intensity, a saturation zone has been formed in the soil layer 0.26 m below the surface of the slope on the 4th day. The gradient of seepage field changes below the saturation zone is relatively large, and the distribution of seepage field is relatively dense. At this time, the entire seepage field distribution is in the form of dense middle and sparse at both ends. On the 6th day, the saturation zone continues to develop downward to the soil layer 0.5 m below the surface of the slope, and the unit gradient of seepage field

continues to increase, which is related to the soil permeability coefficient; The preliminary variation pattern of the seepage field under the condition of moderate rain with a duration of 45 mm/d for 10 days is basically the same as that under heavy rain conditions. However, on the 10th day, the distribution form of the seepage field changes from sparse dense to sparse dense. This is because the surface rainwater on the slope has reached deeper soil layers after long-term subsurface flow.

Through comprehensive analysis of on-site testing and calculation results, it can be concluded that: (1) the main areas of deep slope displacement are located in the K738+900~K739+038 section; (2) The surface displacement monitoring results show that the surface displacement of the slope has developed to a certain extent at present, and the displacement of K738+900~K739+038 section is relatively large, which is speculated to be affected by the recent rainstorm; (3) The settlement monitoring results indicate that there is little change in settlement at K739+040, K739+020, and K738+980 measuring points; (4) There may be two potential sliding surfaces in the K738+995 section. The deep sliding surface is 12 m below the first level platform and 11 m below the third level platform, basically along the interface between sandy clay and completely weathered Andesite porphyrite. The shallow sliding surface is located at a depth of 8 m below the first level platform and 4 m below the third level platform, basically within the sandy cohesive soil layer; The potential sliding surface of K738+910 section is located at a depth of 7 m below the first level platform and 3 m below the third level platform; There may be two potential sliding surfaces in K738+658 section, one is located at the interface between silty clay and sandy clay (9 m below the top of cutting), and the other is mainly located at the interface between sandy clay and completely weathered Andesite porphyrite; (5) The surface layer of the slope is silty clay and sandy clay, and the underlying layer is fully strongly weathered Andesite porphyrite and moderately weathered Dacite. Due to the recent continuous heavy rainfall, the moisture content of the surface soil of the slope gradually increases and tends to become saturated, increasing the self weight of the slope soil and reducing its shear strength, thereby reducing the stability of the slope and inducing deformation and instability.

## **5 Conclusion**

This study is based on a highway slope project in northern Guangdong, and explores the impact of rainfall infiltration on the stability of high slopes.

Firstly, on-site monitoring of surface settlement, deep layer settlement, and other slope displacements was carried out on high slopes. The monitoring data was processed and analyzed to establish a soil high slope displacement prediction model and provide early warning and prediction for high slopes; Subsequently, based on the BC theory, Green Ampt was improved, and an analytical formula for the slope safety coefficient considering the redistribution of wet layers during rainfall was derived. A fluid solid coupling numerical calculation model considering the seepage characteristics of the slope was established. Through numerical simulation, the migration of pore water in the slope and the evolution of slope displacement under different rainfall intensities were studied. The main research conclusions are as follows:

- (1) The groundwater level on the slope is prone to rapid increase in continuous heavy rainfall weather, resulting in saturation of the rock and soil on the slope, and a rapid decrease in the shear strength of the rock and soil, leading to the occurrence of slope diseases; The slope top is relatively flat and the surface runoff conditions are poor. A large amount of surface water replenishes groundwater, leading to the occurrence of slope diseases;
- (2) The height of the slope is relatively high. After excavation, the deformation of the slope further opens the rock and soil joint fissures, forming vertical and horizontal water channels, providing favorable conditions for the rapid infiltration of surface water to recharge groundwater. The groundwater is affected by the relative impermeability of weak interlayers and the high content of clay minerals, resulting in a slower discharge and faster rise of the groundwater level. This increases the dynamic and static water pressure of the landslide body, reduces the effective stress of the landslide body, and causes slope diseases.
- (3) The surface displacement monitoring results show that the surface displacement of the slope has developed to a certain extent at present, and the displacement of K738+900~K739+038 section is relatively large, which is speculated to be affected by the recent rainstorm; There may be two potential sliding surfaces in the K738+995 section.
- (4) Due to the recent continuous heavy rainfall, the moisture content of the surface soil of the slope gradually increases and tends to become saturated, increasing the self weight of the slope soil and reducing its shear strength, thereby reducing the stability of the slope and inducing deformation and instability.

## Acknowledgements

This work was supported by “Study on Slope Safety Risk Assessment System and prevention and Control Countermeasures of operating expressway (2022-MS1-025)”.

## References

- [1] Van Genuchten M T. A closed-form equation for predicting the hydraulic conductivity of unsaturated soils[J]. Soil Science Society of America Journal, 1980, 44(5): 892–898.
- [2] Li A G, Yue Z Q, Tham L G, et al. Field-monitored variations of soil moisture and matric suction in a saprolite slope[J]. Canadian Geotechnical Journal, 2005, 42(1): 13–26.
- [3] He Z B, Zhao W Z, Liu H, et al. The response of soil moisture to rainfall event size in subalpine grassland and meadows in a semi-arid mountain range: a case study in northwestern China’s Qilian Mountains[J]. Journal of Hydrology, 2012, 420/421: 183–190.
- [4] Wei Yangyang, Guo Huidi, Zhang Siyi, Li Jingyuan, et al. Bionic Mechanical Analysis of Dragonfly Wings: The Feasibility of Mesh Combination to Improve Structural Stiffness [J]. European Journal of Computational Mechanics, 2022, 31(4): 459–504.
- [5] Leung F T Y, Yan W M, Hau B C H, et al. Root systems of native shrubs and trees in Hong Kong and their effects on enhancing slope stability[J]. CATENA, 2015, 125: 102–110.
- [6] Leung AK, Kamchoom V, Ng C W W. Influences of root-induced soil suction and root geometry on slope stability: a centrifuge study[J]. Canadian Geotechnical Journal, 2017, 54(3): 291–303.
- [7] Wang Taiheng, Li Wei, Chen Meng, Liu Bin, Wang Jun. Analysis of Factors Influencing Mechanical Properties of Corrugated Steel Based on Entropy Method [J]. European Journal of Computational Mechanics. 2022, 31(4): 539–554.
- [8] Xing X G, Ma X. Simplification of the Gardner model: effects on maximum upward flux in the presence of a shallow water table[J]. Hydrogeology Journal, 2018, 26(4): 1117–1122.
- [9] Chirico G B, Borgam T, Rigon T. Role of vegetation on slope stability under transient unsaturated conditions[J]. Procedia Environmental Sciences, 2013, 19: 932–941.

- [10] Navadeh, N., Goroshko, I. O., Zhuk, Y. A., Fallah, A. S. Approximate Mode-based Simulation of Composite Wind Turbine Blade Vibrations using a Simplified Beam Model [J]. *European Journal of Computational Mechanics*. 2019, 28(4): 307–324.
- [11] Soma A S, Kubota T, Mizuno H. Optimization of causative factors using logistic regression and artificial neural network models for landslide susceptibility assessment in Ujung Loe Watershed, South Sulawesi Indonesia[J]. *Journal of Mountain Science*, 2019, 16(2): 383–401.
- [12] Tsai T L, Chiang S J. Modeling of layered infinite slope failure triggered by rainfall[J]. *Environmental Earth Sciences*, 2012, 68(5): 1429–1434.
- [13] Sharifi, Hamid. Analytical Solution for Thermoelastic Stress Wave Propagation in an Orthotropic Hollow Cylinder [J]. 2022, 31(2): 239–273.
- [14] Cho S E. Surficial Stability Analysis by the Green-Ampt Infiltration Model with Bedrock Boundary Condition[J]. *Korean Society of Hazard Mitigation*, 2015, 15(1): 131–142.
- [15] Shao W, Bogaard T A, Bakker M, et al. Quantification of the influence of preferential flow on slope stability using a numerical modelling approach[J]. *Hydrology and Earth System Sciences*, 2015, 19(5): 2197–2212.
- [16] Shao W, Ni J J, Leung A K, et al. Analysis of plant root-induced preferential flow and pore water pressure variation by a dual-permeability model[J]. *Canadian Geotechnical Journal*, 2017, 54(11): 1537–1552.
- [17] Wu L Z, Zhang L M, Huang R Q. Analytical solution to 1D coupled water infiltration and deformation in two-layer unsaturated soils[J]. *International Journal for Numerical and Analytical Methods in Geomechanics*, 2012, 36(6): 798–816.
- [18] Liu Run, Liang Chao. Study of the bearing capacity at the variable cross-section of a riser-surface casing composite pile[J]. *China Ocean Engineering*, 2021, 35(2): 262–271.
- [19] Shao W, Yang Z J, Ni J J, et al. Comparison of single and dual-permeability models in simulating the unsaturated hydro-mechanical behavior in a rainfall-triggered landslide[J]. *Landslides*, 2018, 15(12): 2449–2464.
- [20] Zhang X, Li P, Li Z B, et al. Characteristics and formation mechanism of the July 25, 2013, Tianshui group-occurring geohazards[J]. *Environmental Earth Sciences*, 2017, 76(5): 219.
- [21] Bai H L, Feng W K, Yi X Y, et al. Group-occurring landslides and debris flows caused by the continuous heavy rainfall in June 2019 in Mibei

- village, Longchuan County, Guangdong Province, China[J]. *Natural Hazards*, 2021, 108(3): 3181–3201.
- [22] Michel G P, Kobiyama M, Goerl R F. Comparative analysis of SHAL-STAB and SINMAP for landslide susceptibility mapping in the Cunha River basin, southern Brazil[J]. *Journal of Soils and Sediments*, 2014, 14(7): 1266–1277.
- [23] Sammartino, Stéphane, Lissy A S, Bogner C, et al. Identifying the Functional Macropore Network Related to Preferential Flow in Structured Soils[J]. *Vadose Zone Journal*, 2017, 14(10).
- [24] Wang Ding-jian, Tang Hui-ming, Zhang Ya-hui, et al. An improved approach for evaluating the time-dependent stability of colluvial landslides during intense rainfall[J]. *Environmental Earth Sciences*, 2017, 76(8): 321.
- [25] Sajjan A K, Gyasi-Agyei Y, Sharma R H. Rainfall runoff modelling of railway embankment steep slopes[J]. *Hydrological Sciences Journal*, 2013, 58(5): 1162–1176.
- [26] Liu Zi-zhen, Yan Zhi-xin, Duan Jian, et al. Infiltration regulation and stability analysis of soilslope under sustained and small intensity rainfall[J]. *Journal of Central South University*, 2013, 20(9): 2519–2527.
- [27] Ng C W W, Shi Q. A numerical investigation of the stability of unsaturated soil slopes subjected to transient seepage[J]. *Computer and Geotechnics*, 1998, 22(1): 1–28.
- [28] Godt Jonathan W, Şener-Kaya Başak, Lu Ning, et al. Stability of infinite slopes under transient partially saturated seepage conditions[J]. *Water Resources Reserch*, 2012, 48(5): W05505.
- [29] Yao Wen-min, Li Chang-dong, Zhan Hong-bin, et al. Time-dependent slope stability during intense rain-fall with stratified soil water content[J]. *Bulletin of Engineering Geology and the Environment*, 2019, 78(7): 4805–4819.
- [30] Griffiths D V, Huang J S, Fenton G A. Probabilistic infinite slope analysis[J]. *Computers and Geotechnics*, 2011, 38(4): 577–584.
- [31] Cai J S, Yeh T J, Yan E C, et al. Uncertainty of rainfall-induced landslides considering spatial variability of parameters[J]. *Computers & Geotechnics*, 2017, 87: 149–162.
- [32] Santoso A M, Phoon K K, Quek S T. Effects of soil spatial variability on rainfall-induced landslides[J]. *Computers & Structures*, 2011, 89(11–12): 893–900.

- [33] Li D Q, Qi X H, Phoon K K, et al. Effect of spatially variable shear strength parameters with linearly increasing mean trend on reliability of infinite slopes[J]. *Structural Safety*, 2014, 49(1): 45–55.
- [34] Gavin Kenneth, Xue Jianfeng. A simple method to analyze infiltration into unsaturated soil slopes[J]. *Computers and Geotechnics*, 2008, 35(2): 223–230.
- Tsai Yi-zhih, Liu Yu-tung, Wang Yung-li, et al. Effects of the grain size on dynamic capillary pressure and the modified Green-Ampt model for infiltration[J]. *Volume Geofluids*, 2018, (2): 1–11.
- [35] Li X, Gaudin C, Tian Y, et al. Effect of perforations on uplift capacity of skirted foundations on clay[J]. *Canadian Geotechnical Journal*, 2014, 51(3): 322–331.
- Chen R, Gaudin C, Cassidy M J. Investigation of the vertical uplift capacity of deep-water mud mats in clay[J]. *Canadian Geotechnical Journal*, 2012, 49(7): 853–865.

## Biographies



**Lu Hao** received the doctor's degree in engineering from Chang'an University in 2018. He is currently working as an engineer at the Department of geotechnical engineering of Guangdong Transportation Technology Testing Co., Ltd. His research areas and directions include slope safety monitoring, consulting evaluation, and disaster prevention and research.



**Li Qing** received the master's degree in engineering from Chang'an University in 2006. He is currently working as an senior engineer at the Department of geotechnical engineering of Guangdong Transportation Technology Testing Co., Ltd. His research areas and directions include slope and tunnel safety monitoring, consulting evaluation and maintenance of reinforcement design.



**Li Peijun** received the master's degree in engineering from Chang'an University in 2019. He is currently working as an engineer at the Department of geotechnical engineering of Guangdong Transportation Technology Testing Co., Ltd. His research areas and directions include slope and tunnel safety monitoring system, disaster prevention and mitigation, application of new technology in geotechnical engineering.